Modeling Oscillatory Phase and PhaseSynchronization with Neuronal Excitation andInput Strength in Cortical Network

Article *in* IEEE Access · June 2018

DOI: 10.1109/ACCESS.2018.2845301

CITATION
1

READS
151

3 authors, including:

Fang Wang
Brunel University London
41 PUBLICATIONS **636** CITATIONS

SEE PROFILE

IEEE Access
Multidisciplinary | Rapid Review | Open Access Journal

Modeling Oscillatory Phase and Phase Synchronization with Neuronal Excitation and Input Strength in Cortical Network

DAMING WANG[1], YAORU SUN[1], AND FANG WANG[2]
[1]Department of Computer Science and Technology, Tongji University, Shanghai, China
[2]Department of Computer Science, Brunel University, Uxbridge UB8 3PH, United Kingdom

Corresponding author: Yaoru Sun (e-mail: yaoru@tongji.edu.cn).

This work was supported by the National Natural Science Foundation of China under Grant 61173116 and Grant 91748122.

ABSTRACT Neuronal oscillatory phase is suggested to be associated with feature coding, carrying information for stimulus identity and neuronal activation, while phase synchronization is indicated to be correlated with signal routing, establishing flexible communication structures for neuronal interactions. Recent electrophysiological and computational studies have revealed that oscillatory phase has close relationships with neuronal excitation and input stimulus. To simulate and further investigate these issues, we simulated orientation columns with a spiking neural network and performed spectral computations according to physiological experiments. Besides, six network activity states, pre-stimulus and stimulus periods were introduced in our simulation for both independent and comparative analyses. The simulation results demonstrated that gamma band neuronal oscillations existed in the network and even emerged during pre-stimulus period. An input stimulus orientation, if approximately preferred, could produce smaller and more concentrated oscillatory phases, but relatively stronger phase synchronization. In particular, the oscillatory phase and phase synchronization had quantifiable relationships with neuronal excitation and input strength. With the network activity state transforming gradually from strong oscillation to non-oscillation, the oscillatory phase became more and more scattered and the strength of phase synchronization declined significantly. Their relationships with neuronal excitation and input strength became increasingly unstable, and finally collapsed.

INDEX TERMS Neuronal coherence, neuronal oscillation, pairwise phase consistency PPC, phase synchronization, spike-LFP phase, spiking neural network.

I. INTRODUCTION

Neuronal activities in numerous cortical and subcortical areas [1-4] of various species [4-6] have been regularly observed to exhibit rhythmic dynamics of neuronal oscillation and synchronization in different frequency bands, which are suggested to underlie a large number of cognitive functions, including signal routing [2, 7, 8], feature integration [9, 10], selective attention [11, 12] and memory [4, 13]. Through physiological experiment, theoretical analysis and computational investigation, the perisomatic inhibition from GABA receptor-mediated interneurons has been found to be critical for the generation of neuronal rhythmicity [14, 15]. Neuronal oscillation and synchronization can arise from any network if there exists appropriately balanced connectivity between pyramidal neuron and interneuron [16, 17], whose period or frequency is primarily determined by decay time constant of shunting inhibition [16, 18, 19].

Neuronal oscillatory phase, referred to here as occurrence of neuronal activities relative to concurrent oscillatory cycle, is supposed to support sensory feature coding [17] and has analytical relationships with neuronal excitation and input stimulus. In hippocampus, a phenomenon of theta-phase precession is commonly observed, where spatial information an animal traveled can be encoded in theta phase [20]. Spike phase of a recorded neuron advances earlier and earlier to the peak of theta cycle, because excitatory drive of the spatial information becomes stronger and stronger when the animal traverses through the neuron's receptive field [21]. Based on the theta-phase precession, a gamma cycle hypothesis advocates that the amplitude of excitatory input and the excitation of pyramidal neuron can be converted into a temporal code of phase value, with stronger external input and neuronal excitation leading to earlier spike phases in the gamma cycle [21]. A subsequent electrophysiological

experiment of gamma-phase shifting in visual cortex is consistent with the hypothesis above [22]. The input orientation stimulus determines spike phases, which shift systematically as a function of neuronal activation strength. Preferred orientation and stronger neuronal activation can give rise to earlier spikes and smaller phases [22].

The following theoretical and computational investigations are in line with the previous hypothesis and experiments about the relationship of oscillatory phase. A computational study confirms that a spike phase can encode stimulus strength in the cortical network, where the spike phase varies from the late to the earlier part of the oscillation cycle when an external input of depolarizing current increases [23]. Another computational study demonstrates that the spike phase of a given neuron decreases when the amplitude of a sinusoidal synaptic input increases [24].

Furthermore, several evidences have been found to support the role of oscillatory phase in encoding of cognitive information. In visual cortex, neurons in anaesthetized macaques can encode naturalistic movie stimuli in terms of spike phases rather than only in light of spike counts [25]. In olfactory bulb, electrophysiological recordings of an awake mice illustrate that an individual neuron can encode the timing of optogenetical activation relative to the sniff cycle in both the timing and the amplitude of their responses [26]. In prefrontal cortex, neuronal information about different objects in short-term memory can be coded at distinct phases of underlying oscillations [27]. In hippocampus, it has been indicated that oscillatory phase can encode, retrieve and segregate different types of information [28].

Two aspects in association with oscillatory phase are taken into consideration: phase representation, reflecting neuronal excitation and property of input stimulus, as well as phase synchronization, quantifying the strength of neuronal synchronization or phase coincidence in phase domain. For phase representation, we utilized point spike-LFP (Local Field Potential) phase in our simulating experiment, which computed the phase of spike time point relative to its background LFP oscillations [29]. LFP oscillation generally embodies itself as aggregated synaptic currents and other transmembrane potentials within a group of adjacent neurons, thus spike-LFP coupling indirectly measures neuronal spiking output and synaptic input[29]. Consequently, the spike-LFP phase is appropriate for quantifying relationships of oscillatory phase and phase synchronization with neuronal input strength.

With respect to phase synchronization, it is proposed to quantify the degree to which neuronal spike activities align with their surrounding oscillations [30], and guarantee dynamic and reliable communications among neuronal groups through CTC (Communication through Coherence) mechanism [7, 31]. Thus far, PLV (Phase Locking Value) [32], general coherence measure [5, 19, 33, 34] and PPC (Pairwise Phase Consistency) [29, 35] are three primary approaches for measuring phase synchronization. Unfortunately, statistical estimates of both the PLV and the general coherence measure suffer from significant bias because of variable and uncontrollable sample size. The PPC measure can overcome this bias by implementing computation of vector dot product instead of vector addition operation [35]. Furthermore, a refined PPC measure of point-field $\hat{P}_2$ implements a normalization operation firstly for pairs of separate trials to make itself unbiased by trial numbers and phase-spike count dependency. Besides, it eliminates the dot product operation of oscillatory phase with itself, and only executes the operation across different trials [29]. We adopted the point-field PPC $\hat{P}_2$ measure, hereinafter called PPC2 measure, to quantify phase synchronization in our simulating experiment.

However, up to present, there are not too many computational models to simulate and quantify relationships of oscillatory phase with neuronal excitation and input stimulus strength, especially by means of spectral computation and according to physiological experimental procedure. In particular, the relationship quantification of phase synchronization with neuronal excitation and input strength is even less. Inspired by the gamma-phase shifting experiment [22], we investigated detailed properties of oscillatory phase and phase synchronization, as well as their relationships with neuronal excitation and input strength in six different network activity states. The oscillatory phase was characterized by spike-LFP phase, and the phase synchronization by PPC2 measure. The neuronal excitation was quantified by neuronal firing rate, with the input strength by neuronal synaptic current power and input Poisson rate. Orientation columns in primary visual cortex were approximately simulated by way of a spiking neural network and PING (Pyramidal Interneuron Gamma Model) mechanism [17, 36], which entailed an indispensable component of inhibitory neurons. The purpose of constructing orientation columns was not only because of orientation preference and input orientation stimulus encountered in physiological experiment, but also aiming at studying characteristics of oscillatory phase and phase synchronization in more complicated neural network.

In our simulating experiment, the simulation procedure, stimulus stimulation, data sampling and the subsequent spectral analysis were approximately analogous to the gamma-phase shifting study [22]. For comparison, we explored the neuronal dynamics in six network activity states independently and comparatively, which were modulated by different levels of Gaussian noise [37-39]. Besides, the investigation was also carried out for a pre-stimulus period with no stimulus and a stimulus period with orientation stimulus. Furthermore, we implemented a time-resolved analysis for the evolutions of oscillatory phase and phase synchronization across trial time with a sliding window. Moreover, the simulating investigation could reproduce more data and perform more analyses from multiple viewpoints to supplement data deficiency and condition variations in physiological experiments, for instance, varying spike and

trial numbers for different experiments [35]. Finally, the investigation of oscillatory phase, phase synchronization and especially their relationships with neuronal excitation and input strength is proposed to lay the foundations for cortical computation, including phase-based feature coding, neuronal communication, selective attention.

II. MATERIALS AND METHODS

A. NEURONAL MODEL

A leaky integrate-and-fire model, adapted from [40], was adopted in our simulating experiment, the voltage dynamics of which was according to the following equation:

$$\frac{dV}{dt} = \frac{-g_L(V-V_{rest})+I_{AMPA}+I_{GABA}+I_{bg}}{C_m} + \sigma_n\sqrt{\frac{2}{\tau_n}}\xi(t) \quad (1)$$

where the term V denoted a membrane potential, g_L a membrane leaky conductance, C_m a membrane capacitance, and I_{bg} a constant tonic background current. I_{AMPA} and I_{GABA} depicted excitatory and inhibitory synaptic currents respectively. Besides, $\xi(t)$ described a normalized Gaussian white noise with mean 0 and variance 1 [41], where τ_n was a time constant of the Gaussian noise and σ_n was a varying parameter for modulating neuronal network activity state. Whenever the V surpassed a potential threshold V_{thres}, an action potential was engendered and then passed to all neurons it anatomically connected. Afterwards, the V was reset to a resting potential V_{rest} and kept clamped for a refractory period T_{ref}.

$$I_{AMPA} = g_{AMPA}(V_E - V) \quad (2)$$

$$I_{GABA} = g_{GABA}(V_I - V) \quad (3)$$

$$\frac{dg_{AMPA}}{dt} = -\frac{g_{AMPA}}{\tau_{AMPA}} \quad (4)$$

$$\frac{dg_{GABA}}{dt} = -\frac{g_{GABA}}{\tau_{GABA}} \quad (5)$$

$$g_{AMPA} = g_{AMPA} + \Delta g_{AMPA} \quad (6)$$

$$g_{GABA} = g_{GABA} + \Delta g_{GABA} \quad (7)$$

The evolution of conductance-based synaptic currents, I_{AMPA} and I_{GABA}, obeyed Equations (2) and (3), where g_{AMPA} and g_{GABA} were excitatory and inhibitory synaptic conductance. Correspondingly, V_E and V_I were excitatory and inhibitory reversal potentials. In general, g_{AMPA} and g_{GABA} evolved on the basis of Equations (4) and (5), wherein τ_{AMPA} and τ_{GABA} were excitatory and inhibitory decay time constant. However, upon receiving an action potential, the synaptic conductance evolved in other ways, through Equations (6) and (7). Besides, Δg_{AMPA} and Δg_{GABA} were established by synaptic connection weight between interconnected neurons, to be interpreted in the following sections.

B. MODEL ARCHITECTURE

In general, cortical columns are regarded as fundamental units for cortical organization and have competitive advantages for neuronal computation [17, 42]. Besides, different orientation stimulus elicited distinct neuronal activations and spike phases in the gamma-phase shifting study [22]. Consequently, we constructed a spiking neural network to simulate orientation columns in primary visual cortex. On the left of Fig. 1(a) are 21 groups of Poisson neurons for simulating external thalamic spike inputs, with 2100 Poisson neurons totally, 100 for each Poisson group. From bottom to top on the right of the Fig. 1(a) are consecutively 21 orientation columns. Each column was comprised of 100 excitatory neurons and 25 inhibitory neurons, portrayed by two cuboids, with same color and number. Consequently, the ratio of the excitatory versus the inhibitory neurons was 80% vs. 20%, consistent with experimental and computational evidences [19, 34, 43]. There were 2100 excitatory neurons and 525 inhibitory neurons within the 21 columns in total, all represented by the leaky integrate-and-fire model mentioned above. Furthermore, feedforward and reciprocal synaptic connections were illustrated by arrows, with red and blue ones representing excitatory and inhibitory synaptic connectivity respectively. Apparently, the connections within the 21 orientation columns exhibited PING principle [36].

It has been widely recognized that neurons in visual cortex are sensitive to orientation stimulus and exhibit bell-shape tuning curve of firing rate, firing strongly with preferred orientations [44]. In consequence, both the excitatory and inhibitory neurons in each column were successively assigned with a preferred orientation, with $-\pi/2 + \pi(i-1)/21$ for the i^{th} column. Typically, two far end columns, the 1st and the 21th ones, had similar orientation preference, which gave rise to a ring topology of stimulus sensitivity across columns. Moreover, we also designated the neurons in the 21 Poisson groups with the same preferred orientations as their corresponding orientation columns so as to obtain reliable external spike inputs.

C. SYNAPTIC CONNECTION

Stimulus selectivity, like orientation preference, has been suggested to be brought about by cortical topography and anatomical connectivity [45, 46]. A feedforward model posits that the orientation selectivity simply arises from the thalamic input projection from LGN (Lateral Geniculate Nucleus) to visual cortex [44, 45]. A feedback or recurrent model proposes that the thalamic projection establishes an initial and mild orientation preference, whereas excitatory intracortical interconnectedness and inhibitory interconnection provide an enhanced orientation bias [44, 47]. In our model, the connectivity from the Poisson groups to their corresponding orientation columns was feedforward, one group to one column, responsible for generating an initial orientation preference. Their connection weights W_f were constant and all the same, with a connecting probability $\varepsilon = 20\%$. However, the connection weight within the 21 orientation columns was determined by feature difference of orientation preference

This article has been accepted for publication in a future issue of this journal, but has not been fully edited. Content may change prior to final publication. Citation information: DOI 10.1109/ACCESS.2018.2845301, IEEE Access

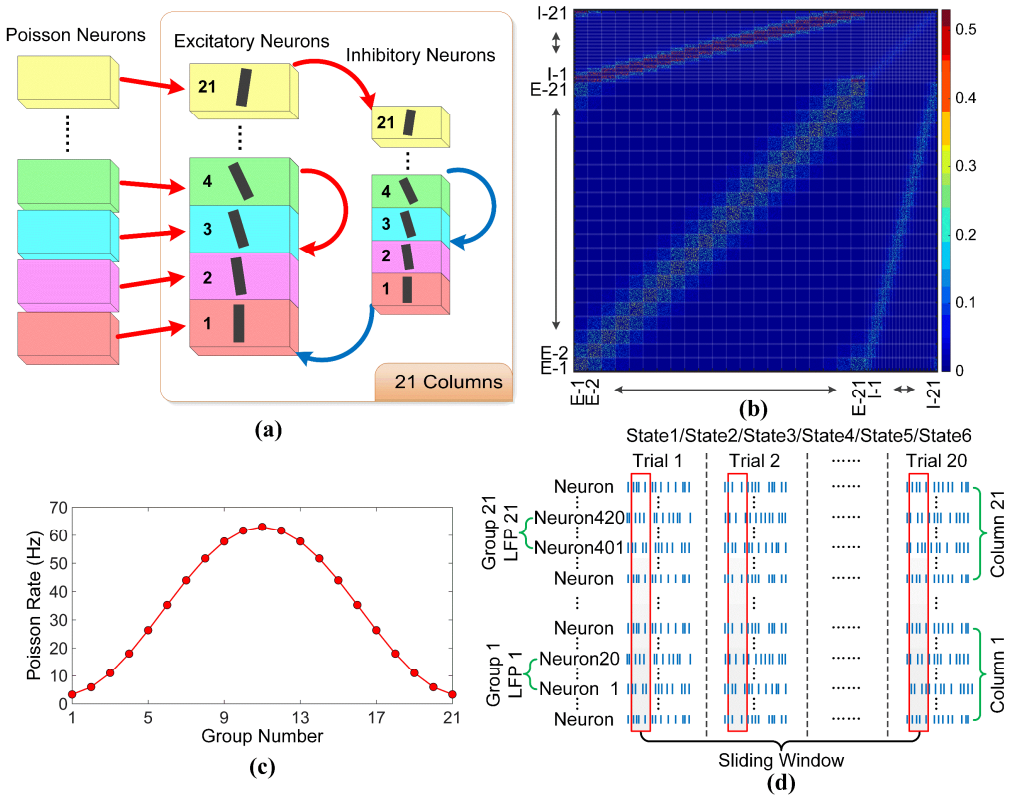

FIGURE 1. Model Architecture and Simulation Procedure. (a) Architecture of neuronal network. The left side is 21 groups of Poisson neurons, and the right is 21 orientation columns, each with a group of excitatory and inhibitory neurons. Black bars with various directions represent preferred orientations for corresponding columns. Red and blue arrows denote excitatory and inhibitory synaptic connections respectively. (b) Connection weight matrix within 21 orientation columns. Column numbers are assigned and duplicated on x- and y- axis, for instance, E-1 and I-1 embodying excitatory and inhibitory neurons from the first column respectively. (c) Poisson rate of 21 Poisson groups. (d) Overview of simulation procedure.

between presynaptic and postsynaptic neurons, which reinforced the orientation preference.

$$W_{ij} = We^{\beta\left[\cos\left(2\left(\theta_{pre}-\theta_{post}\right)\right)-1\right]} \tag{8}$$

where preferred orientations for the presynaptic and postsynaptic neurons were characterized by θ_{pre} and θ_{post}. There were four instances for the parameter W: W_{EE}, W_{EI}, W_{IE}, W_{II}, interpreted as basic connection weights from excitatory to excitatory, excitatory to inhibitory, inhibitory to excitatory, inhibitory to inhibitory neurons respectively. In particular, the parameter W_{IE} was larger than W_{EI} so as to compensate the inhibitory neurons with a small quantity, which gave rise to an appropriate balance between excitation and inhibition in the network [48, 49] (Fig. 1(b)). Besides, a connecting probability $\varepsilon = 20\%$ was employed for the recurrent connectivity as well.

Owing to the same orientation preference, connection weights for an orientation column with itself were strongest, no matter what type of neuronal connectivity (Fig. 1(b)). The connection weights were secondly strongest between nearby columns on account of similar preferred orientations. However, the connection weights were progressively and considerably declined as the feature difference of preferred orientation or spatial distance between columns was increased, in agreement with experimental findings that the connection probability decays with distance [19, 50].

D. AFFERENT POISSON INPUT

The 21 Poisson groups, serving as the role of LGN, supplied external thalamic inputs to orientation columns in visual cortex. The determinant of Poisson rate R_{input} depended solely on the feature difference between the preferred orientation of a Poisson neuron and the actual orientation of input stimulus, inspired from [51].

$$R_{input} = \left[\cos\left(2\left(\theta_{pref} - \theta_{stim}\right)\right) + 1\right] F_{max} \tag{9}$$

wherein the parameter θ_{pref} denoted the preferred orientation of a given Poisson neuron, θ_{stim} the current orientation of input stimulus delivered to the experiment, and F_{max} a maximal firing rate.

E. SIMULATION PROCEDURE

As visible in Fig. 1(d), there are 21 orientation columns upwards successively. In the middle of each column, we continuously selected 20 excitatory neurons as a neuronal

This article has been accepted for publication in a future issue of this journal, but has not been fully edited. Content may change prior to final publication. Citation information: DOI 10.1109/ACCESS.2018.2845301, IEEE Access

group and then recorded their spike timings, synaptic and background currents, from which one LFP channel data was indirectly simulated. Therefore, 420 neurons and 21 LFP channels were recorded altogether, with 20 neurons and one LFP channel corresponding to a microelectrode recording site in a physiological experiment.

In our simulating experiment, we modulated the dynamics of neuronal network by different levels of external Gaussian noise [37-39], and sequentially obtained six network activity states: state1 (σ_n=0.5 mV), state2 (σ_n=1.0 mV), state3 (σ_n=1.5 mV), state4 (σ_n=2.0 mV), state5 (σ_n=2.5 mV) and state6 (σ_n=3.0 mV). However, the network activity state could also be regulated by other types of noise or other parameters, for instance, synaptic time course, synaptic strength and periodic external input [51]. For each activity state, we carried out 20 trials, each composed of a 500 ms pre-stimulus period and a 1500 ms stimulus period. During pre-stimulus period, there were merely Poisson spike trains with a lower rate F_{bg} and a constant background current I_{bg}, for simulation of spontaneous activity in cerebral cortex and maintenance of minimal activity in neuronal network [52]. During stimulus period, nevertheless, a stimulus orientation was presented to simulate drifting gratings. Throughout the experiment, we only imported a constant stimulus orientation, $-\pi/42$, across all 120 trials. It was the preferred orientation of the 11th orientation column, which could result in strong Poisson input and high neuronal excitation for this column. Besides, owing to the effect of response onset transients, we removed the beginning 250 ms and 120 ms data for pre-stimulus and stimulus periods respectively [22]. Then, the Poisson rates of 21 Poisson groups were established by means of Equation (9) (Fig. 1(c)).

In addition, the column network construction, experiment simulation and relevant data recording were based on an open source simulator, a Python package, namely Brian [53]. A time step of 0.1 ms was utilized for numerical Euler integration. The subsequent theoretical computation and spectral analysis were on the basis of a MATLAB toolbox, FieldTrip [54], especially its Spike package [22]. Besides, relevant regression analysis was executed with the aid of SPSS statistics software.

F. LFP SIMULATION

The LFP data was approximately quantified as the sum of several absolute values, including excitatory and inhibitory synaptic currents, as well as tonic background current for excitatory neurons within an adjacent neuronal group [55], revised from [19, 49].

$$LFP = R\left(\sum_{i=1}^{n}\left(|I_{AMPA}| + |I_{GABA}| + |I_{bg}|\right)\right) \quad (10)$$

where the parameter R simulated microelectrode impedance in neurophysiological recordings. The term I_{AMPA} depicted thalamic input current from Poisson spike train, and intracortical excitatory recurrent synaptic current. I_{GABA} exclusively reflected the inhibitory recurrent synaptic current. I_{bg} represented the constant background current. The term n equaled to 20 because 20 neurons constituted a neuronal group for simulating a LFP channel. Besides, the sampling frequencies for spike and LFP signal were 10000 Hz and 1000 Hz respectively, and the LFP signal was bandpass filtered with 0.7-170 Hz. Ultimately, all parameters encountered in our simulation were customized according to Table. 1.

TABLE 1. Default parameter configuration.

Parameter	Value	Parameter	Value
g_L	10 nS	τ_{GABA}	10 ms
C_m	250 pF	β	5
I_{bg}	270 pA	ε	20%
σ_n	0.5/1.0/1.5/2.0/2.5/3.0 mV	W_f	0.15
τ_n	25 ms	W_{EE}	0.29
V_{thres}	-45 mV	W_{EI}	0.2
V_{rest}	-65 mV	W_{IE}	0.53
T_{ref}	5 ms	W_{II}	0.1
V_E	0 mV	F_{max}	30 Hz
V_I	-75 mV	F_{bg}	3 Hz
τ_{AMPA}	5 ms	R	1.0 MΩ

G. SPIKE-LFP PHASE

Around each spike time point of a given neuron, we cut out 20 LFP segments with the exception of the one within the same orientation column, the centers of which were all in accordance with the spike time point. Specially, we adopted varying lengths of LFP segment for different frequencies, with five periodicities for each frequency, for example, a 100 ms length LFP segment for a 50 Hz frequency. Through Discrete Fourier Transform with a Hanning window, all LFP segments were decomposed into spike-triggered LFP spectrum $X_i(f)$ at a specific frequency, described in Equation (11) [22].

$$X_i(f) = \sum_t^T w(t)x_i(t)e^{-2\pi jft} \quad (11)$$

$$\bar{X}_i(f) = \frac{1}{20}\sum_{j=1}^{20}\frac{X_i^j(f)}{\left|X_i^j(f)\right|} \quad (12)$$

$$\Theta_i = angle\left(\bar{X}_i(f)\right) \quad (13)$$

$$\bar{\Theta} = angle\left(\sum_i^N \bar{X}_i(f)\right) \quad (14)$$

wherein $w(t)$ was the Hanning window, $x_i(t)$ a LFP segment data centered around the ith spike. Then the magnitudes of the spectrum were eliminated through normalization across 20 LFP channels by way of Equation (12) [22]. The term $X_i^j(f)$ represented the spike-triggered LFP spectrum from the jth LFP channel and the ith spike of a certain neuron. Afterwards, we could easily derive, at a particular frequency, a point spike-LFP phase by means of Equation (13). Then a spike-LFP phase for an individual neuron or a neuronal group in each network activity state could be obtained through Equation (14) across all 20 trials. The function angle is a

This article has been accepted for publication in a future issue of this journal, but has not been fully edited. Content may change prior to final publication. Citation information: DOI 10.1109/ACCESS.2018.2845301, IEEE Access

classical MATLAB function for returning the phase angle of input complex data.

H. PPC2 MEASURE

With regard to the PPC2 measure adopted in our simulating experiment, we firstly classified the obtained point spike-LFP phase Θ_i into $\Theta_{k,m}$ according to its trial number, $m \in \{1, \cdots, M\}$, with $M = 20$ depicting the trial number for a network activity state, whereas $k \in \{1, \cdots, N_m\}$, with N_m describing the spike number emitted in the m[th] trial. Therefore, the term $\Theta_{k,m}$ represented the k[th] point spike-LFP phase from the m[th] trial for a given neuron. The term $U_{k,m} = (\cos(\Theta_{k,m}), \sin(\Theta_{k,m}))$ was a vector representation for a point spike-LFP phase. Subsequently, we could quantify the precision of phase synchronization for an individual neuron in six network activity states by virtue of Equation (15) [29].

$$PPC2 = \frac{1}{|\mathcal{M}|(|\mathcal{M}|-1)} \sum_{m \in \mathcal{M}} \sum_{l \in \mathcal{M}} \left(\frac{\sum_{k=1}^{N_m} \sum_{j=1}^{N_l} U_{k,m} \cdot U_{j,l}}{N_m N_l} \right) \quad (15)$$

where $\mathcal{M}$ was defined as $\{m \in \{1, \cdots, M\}; N_m > 0\}$, with $|\mathcal{M}|$ meaning the number of trials having at least one spike. The operator $\cdot$ was a dot product operation. The PPC2 measure was unbiased by trial number and spike number because the sum of the dot product of point spike-LFP phases for each pair of separate trials was averaged firstly.

I. TIME-RESOLVED ANALYSIS

Apart from the general computation and analysis from the perspective of the whole trial time, we carried out a time-resolved spectral analysis with a sliding window, portrayed by red rectangles in Fig. 1(d). The sliding window, 75 ms in width, moved with a step of 10 ms. When the sliding windows moved to a certain time point of 20 trials, there were 20 segments of spike and LFP data, one segment for each trial. The length of segments was equivalent to the width of the sliding window. As the windows moved to a new time point, another new 20 segments of spike and LFP data were generated. As a matter of fact, the time-resolved analysis rendered the current 20 trials of numerical recording data to a continuous series of 20 short-time trials of data, all with a length of 75 ms. Then we launched computations of spike-LFP phase and PPC2 value for the obtained series of segment data to investigate the evolvement of oscillatory phase and phase synchronization across trial time for all six network activity states.

III. RESULTS

A. SPIKE ACTIVITY AND LFP SIGNAL

In this section, we investigated neuronal spike activity, LFP signal and LFP power spectrum, but only some of the LFP channels and network activity states were illustrated. The spike raster of Poisson neuron (Pois) during pre-stimulus period was considerably sparse and uniform (Fig. 2(a)). As for Poisson neuron during stimulus period, the distribution of spike raster across neurons was consistent with Poisson rates of 21 Poisson groups determined previously (Fig. 1(c)). During stimulus period, both excitatory (Exc) and inhibitory (Inh) individual neurons exhibited irregular spike activities, whereas their population neurons displayed rhythmicity and collective oscillations, in accordance with in vivo [11, 17] and numerical evidences [19, 51]. The oscillations originated mechanistically from PING structure including recurrent interplay between excitatory and inhibitory neurons [17]. As the parameter σ_n of Gaussian noise increased, the network activity states transformed from strong oscillation to weak oscillation or non-oscillation. Besides, the frequencies of neuronal oscillations during stimulus period were greater than

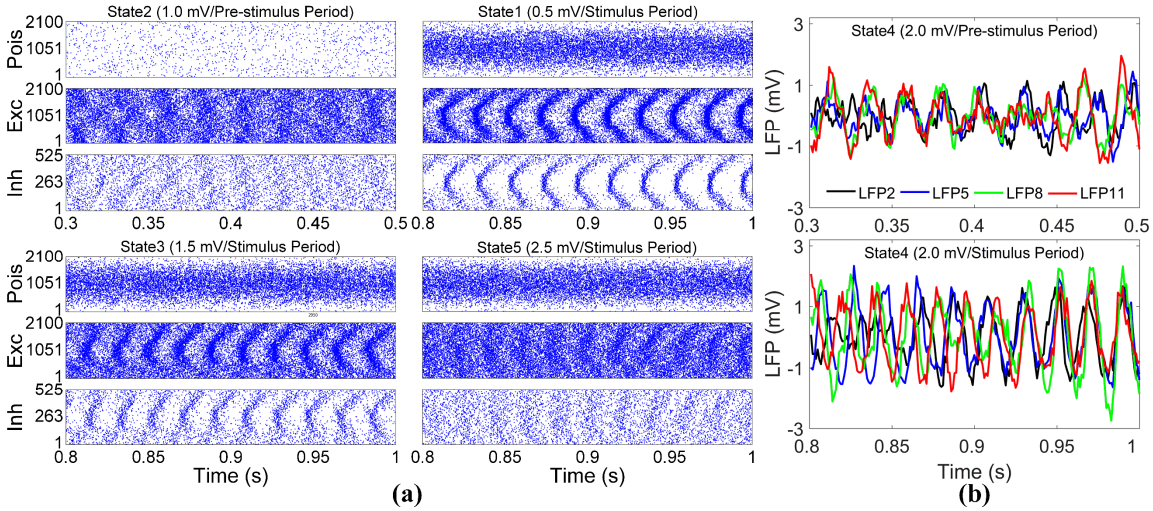

FIGURE 2. Neuronal Spike Activity and LFP Signal. (a) Spike raster plots for all neurons in the neuronal network within a 200 ms interval for state2 during pre-stimulus period, as well as for state1, state3 and state5 during stimulus period. Pois represents Poisson neurons, Exc and Inh denoting excitatory and inhibitory neurons in 21 orientation columns respectively. (b) Time series of four LFP signals from the 2nd, the 5th, the 8th and the 11th orientation columns within a 200 ms interval for state4 during pre-stimulus and stimulus periods.

This article has been accepted for publication in a future issue of this journal, but has not been fully edited. Content may change prior to final publication. Citation information: DOI 10.1109/ACCESS.2018.2845301, IEEE Access

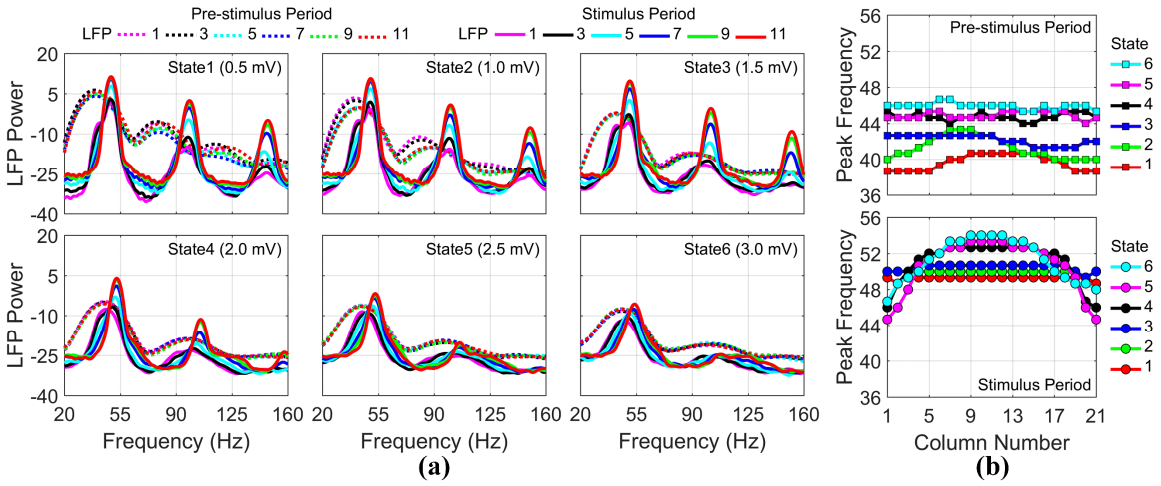

FIGURE 3. LFP Power Spectra and Peak Frequencies of LFP Power. (a) Power spectra of six LFP signals for six network activity states during pre-stimulus period (dotted line) and stimulus period (solid line). The six LFP signals are from the 1st, the 3rd, the 5th, the 7th, the 9th, and the 11th orientation columns respectively. (b) Peak frequencies of LFP power spectrum from 21 orientation columns for six network activity states during pre-stimulus and stimulus periods.

those during pre-stimulus period, which, however, were all within gamma range. The oscillatory frequency was primarily dependent on decay time constant of inhibitory synaptic conductance and external input [49].

In addition, during stimulus period, oscillation peaks of both excitatory and inhibitory spike raster from different orientation columns were fairly heterogeneous (Fig. 2(a)). The oscillation peak from the 11th column emerged firstly and then the upward and downward columns in succession, with the 1st and the 21th columns being the last ones. Because neurons from the 11th column received the strongest Poisson spike inputs and were further supplemented by strong excitatory connectivity within the column itself. The peak differences of spike raster or neuronal oscillations across columns may lay the foundations for producing different oscillatory phases. Besides, as parameter σ_n was increased, the oscillatory peak differences across columns became smaller and smaller.

For LFP signal, owing to slightly consistent oscillations of excitatory spike raster across columns during pre-stimulus period, the LFP signals within this period had roughly similar oscillatory peaks and amplitudes (Fig. 2(b)). However, during stimulus period, the peaks of LFP signals were largely different, with the 11th, the 8th, the 5th and the 2nd channels one after another for most of the 200 ms interval. It was in agreement with excitatory oscillations of spike raster illustrated above. Besides, it has been revealed in a computational simulation that spike discharges with a higher probability around the trough of LFP oscillations [19]. In consequence, it is reasonable that the peak differences of LFP signals and spike location specificity provide a reliable account for the generation of different oscillatory phases and then different precisions of phase synchronization.

It has been observed that inhibitory decay time constant τ_{GABA} and stimulus contrast are capable of modulating peak frequencies [49]. The oscillatory frequency increases monotonically with stimulus contrast [56, 57], whose changes are regularly modeled as variations in the rate of spike train [49]. In our simulating experiment, we measured LFP power spectra with a Welch method. The shapes of simulated LFP powers are in agreement with several physiological and computational studies [19, 37, 57] (Fig. 3(a)). The peak frequencies of power spectra were not only consistent with the frequencies of raster oscillations and LFP oscillations, but also within gamma range. From state1 to state6 during pre-stimulus period, the peak frequencies of LFP power became larger and larger, however, remaining similar across 21 columns (Fig. 3(b)). From state1 to state6 during stimulus period, the differences of the peak frequencies across columns became increasingly larger. Moreover, it has been believed that phase coherence is generally highest around peak frequency of power spectra [49, 58]. Henceforth, the following investigations of spike-LFP phase and PPC2 value were primarily carried out around the peak frequencies of LFP power, unless the whole spectrum analysis was illuminated if necessary.

B. NEURONAL FIRING RATE AND SYNAPTIC CURRENT POWER

We computed neuronal firing rate and synaptic current power for both 420 individual neurons and 21 neuronal groups. The firing rate denoted neuronal excitation, and the synaptic current power indirectly represented neuronal input strength. The synaptic current power was obtained through Welch's power spectral density estimate for the sum of excitatory synaptic current and background current projecting to a neuron. During pre-stimulus period, the excitatory spike raster across orientation columns oscillated with similar densities, which implicitly suggested similar neuronal excitations and firing rates. Despite the firing rates of the 420 individual neurons for this period varied a lot, their distributions across

This article has been accepted for publication in a future issue of this journal, but has not been fully edited. Content may change prior to final publication. Citation information: DOI 10.1109/ACCESS.2018.2845301, IEEE Access

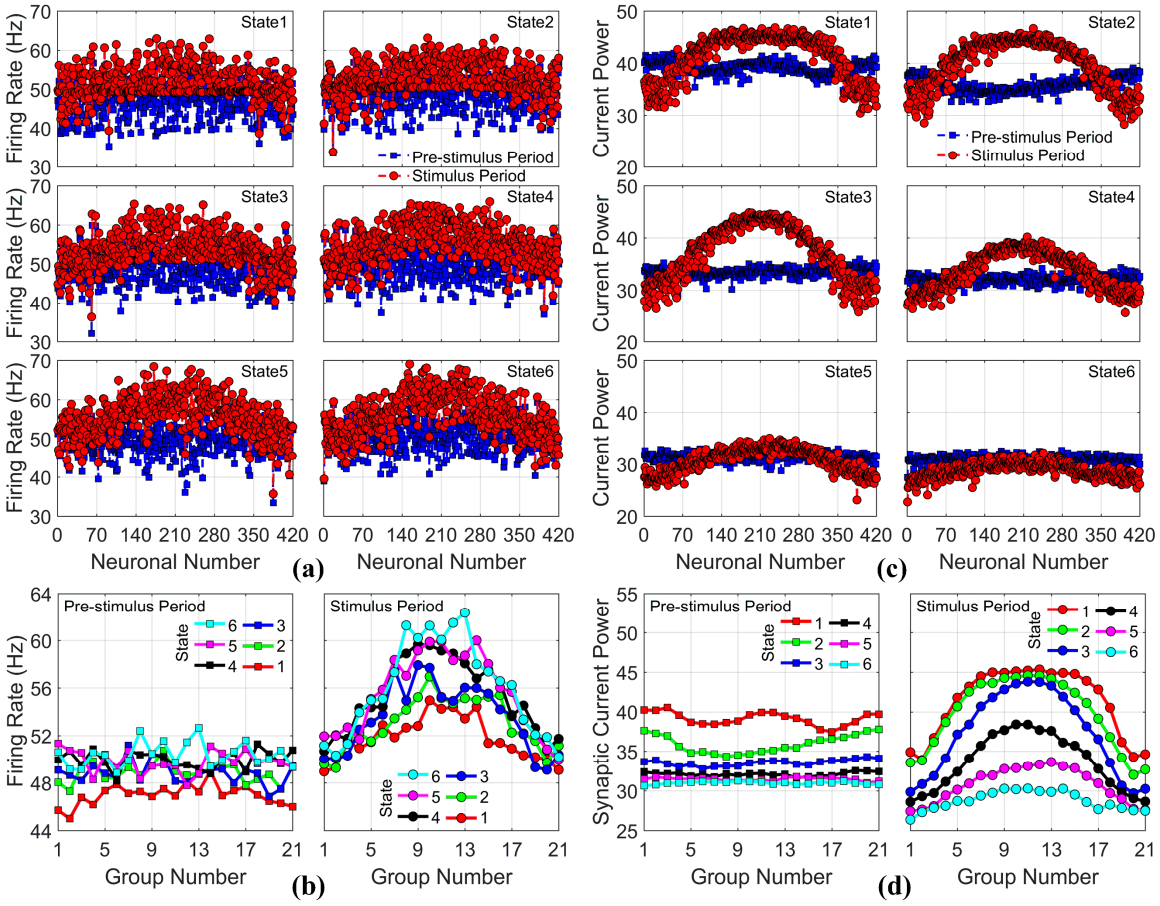

FIGURE 4. Neuronal Firing Rate and Synaptic Current Power. (a) Firing rates of 420 individual neurons for six network activity states during pre-stimulus and stimulus periods. (b) Similar to (a), but for firing rates of 21 neuronal groups. (c) Synaptic current power of 420 individual neurons for six network activity states during pre-stimulus and stimulus periods. (d) Similar to (c), but for synaptic current power of 21 neuronal groups.

columns were roughly similar (Fig. 4(a)). Besides, the firing rates of 21 neuronal groups across columns within this period were relatively flat (Fig. 4(b)). Owing to the same Poisson rate of spike inputs and similar neuronal activities across excitatory neurons and orientation columns during pre-stimulus period, the synaptic current powers were comparatively stationary for both 420 individual neurons (Fig. 4(c)) and 21 neuronal groups (Fig. 4(d)). From state1 to state6 for both individual neurons and neuronal groups during this period, the firing rates became slightly larger and larger, whereas the synaptic current powers became increasingly smaller.

During stimulus period, the spike raster from the middle orientation columns had relatively greater densities, which in consequence indicated stronger neuronal excitations and higher firing rates. Though to some extent do the firing rates of 420 individual neurons fluctuated, there were nevertheless slightly higher firing rates for neurons from the middle columns (Fig. 4(a)). In the case of neuronal groups, the firing rates across groups were apparently much more distinct than those across single neurons, with values from the middle groups larger than the ones from other groups (Fig. 4(b)). The synaptic current powers of both individual neurons and neuronal groups were strongest for the middle columns, and then decreased gradually towards two end columns (Fig. 4(c) and Fig. 4(d)). From state1 to state6 for both individual neurons and neuronal groups, the firing rates became relatively greater and greater, with their differences across neurons or groups becoming increasingly sharper. However, the synaptic current powers became smaller and smaller, which also became growingly similar across neurons and groups. Moreover, no matter firing rate or synaptic current power, single neuron or neuronal group during stimulus period, the tuning curves of both firing rate and synaptic current power guaranteed orientation selectivity in visual cortex [44, 45], also compatible with the Poisson rates of 21 Poisson groups (Fig. 1(c)).

C. SPIKE-LFP PHASE

In this section, we analyzed spike-LFP phase in both polar coordinates and Cartesian coordinates. For relatively strong oscillatory state1 and state2 during pre-stimulus period, spike-LFP phases of 420 individual neurons were comparatively flat and similar, with the exception of several deviating data (Fig. 5(b)). They were considerably concentrated in each orientation column, with lower standard deviation values (Fig. 5(a, b, d)). Spike-LFP phases of 21 neuronal groups during this

This article has been accepted for publication in a future issue of this journal, but has not been fully edited. Content may change prior to final publication. Citation information: DOI 10.1109/ACCESS.2018.2845301, IEEE Access

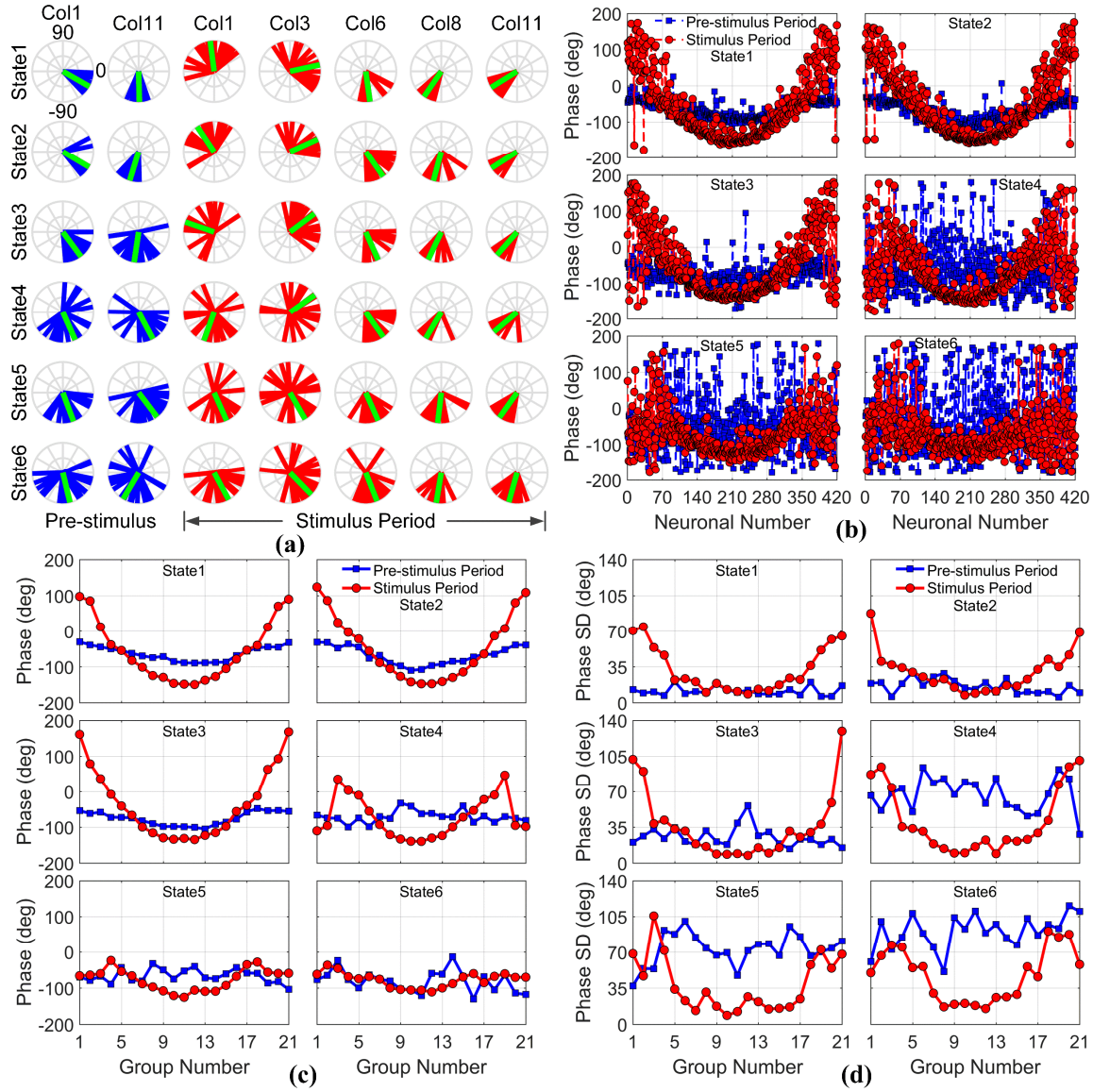

FIGURE 5. Spike-LFP Phase. (a) Spike-LFP phases in polar coordinates for six network activity states, one row for one state and one column for one orientation column (Col1 means the 1st orientation column). One polar coordinate has 21 spike-LFP phases, with blue bar for pre-stimulus period and red bar for stimulus period. Green bar represents spike-LFP phase for a neuronal group. The radial length equals to unit length, because amplitude is normalized. (b) Spike-LFP phases of 420 individual neurons for six network activity states during pre-stimulus and stimulus periods. (c) Similar to (b), but for spike-LFP phases of 21 neuronal groups. (d) Standard deviation (SD) of spike-LFP phases for 21 neuronal groups in six network activity states during pre-stimulus and stimulus periods.

period for these oscillatory states possessed similar attributes (Fig. 5(c)). As the parameter σ_n was increased, spike-LFP phases of individual neurons during pre-stimulus period became more and more scattered, especially for weak oscillation or non-oscillation from state4 to state6.

For relatively strong oscillation from state1 to state3 during stimulus period, spike-LFP phases of individual neurons from the 11th orientation column were smallest, typically smaller than the ones during pre-stimulus period (Fig. 5(b)). However, as feature difference of preferred orientation or spatial distance relative to the 11th column increased, the spike-LFP phases from the leftward and rightward columns increased progressively, and the ones from two-side columns were generally larger than those during pre-stimulus period. Besides, the spike-LFP phases from the 11th column were most concentrated, nevertheless the ones from other columns leftwards and rightwards became more and more scattered (Fig. 5(a, b, d)). The spike-LFP phases of neuronal groups for these states have analogous properties (Fig. 5(c)). For weak oscillation or non-oscillation from state4 to state6 during stimulus period, the spike phases of individual neurons, especially the ones from two-side columns shifted extensively. Furthermore, although neurons within the same orientation column had identical orientation preference, similar

This article has been accepted for publication in a future issue of this journal, but has not been fully edited. Content may change prior to final publication. Citation information: DOI 10.1109/ACCESS.2018.2845301, IEEE Access

connectivity and analogous Poisson input, there were still variations in their spike-LFP phases within the column. Typically, the larger difference between preferred orientation and actual input orientation, the more variable the spike phases were.

The input orientation was the same as the preferred orientation of the 11th column, it therefore provided the strongest Poisson input for this column. Supplemented with strong lateral connections within the column, the excitatory neurons from this column fired firstly and then iteratively engendered roughly synchronous activities of inhibitory neurons, which in turn exerted shunting inhibition over the entire 21 orientation columns to prevent their neurons from spiking [59]. As a consequence of similar preferred orientations and secondarily strong Poisson input, excitatory neurons from the 10th and the 12th columns could overcome the shunting inhibition secondly, and likewise generated rhythmic and synchronized inhibitions to prohibit excitatory neurons of other columns from discharging. Afterwards, similar phenomenon emerged in the 9th and the 13th columns, with the 1st and the 21th columns the last ones. Therefore, there actually existed a time sequence of rhythmic inhibitions for 21 orientation columns, which was primarily responsible for the occurrence of neuronal oscillations for the 21 columns one after another. This was the reason why the spike-LFP phases of individual neurons or neuronal groups across columns were considerably different and in a time order during stimulus period.

D. PAIRWISE PHASE CONSISTENCY PPC2

The PPC2 measure utilized in our simulating experiment is referred to as a temporal approach for measuring the strength of phase synchronization and quantifying the degree to which point spike-LFP phases coincide with specific locations of LFP oscillations. For six network activity states during pre-stimulus period, the PPC2 values across 420 neurons were similar and quite low (Fig. 6). For strong oscillatory state1 during stimulus period, most of neurons from the middle orientation columns had greater PPC2 values, which however declined gradually toward two-side columns. Besides, the significant region of PPC2 values was primarily within a range from 45 Hz to 95 Hz, which belonged to a gamma frequency band, matching well with a set of physiological and simulating investigations [5, 22, 52]. From state1 to state6 during stimulus period, the middle region with higher PPC2 values became considerably narrower and narrower.

Then, we investigated the PPC2 values of 420 individual neurons around the peak frequencies of LFP power (Fig. 7(a)). For six activity states during pre-stimulus period, most of 420 neurons came up with comparatively lower PPC2 values, except for a few departing points. For state1 during stimulus period, the PPC2 values for most of the neurons from the 11th orientation columns were relatively larger, the ones for the

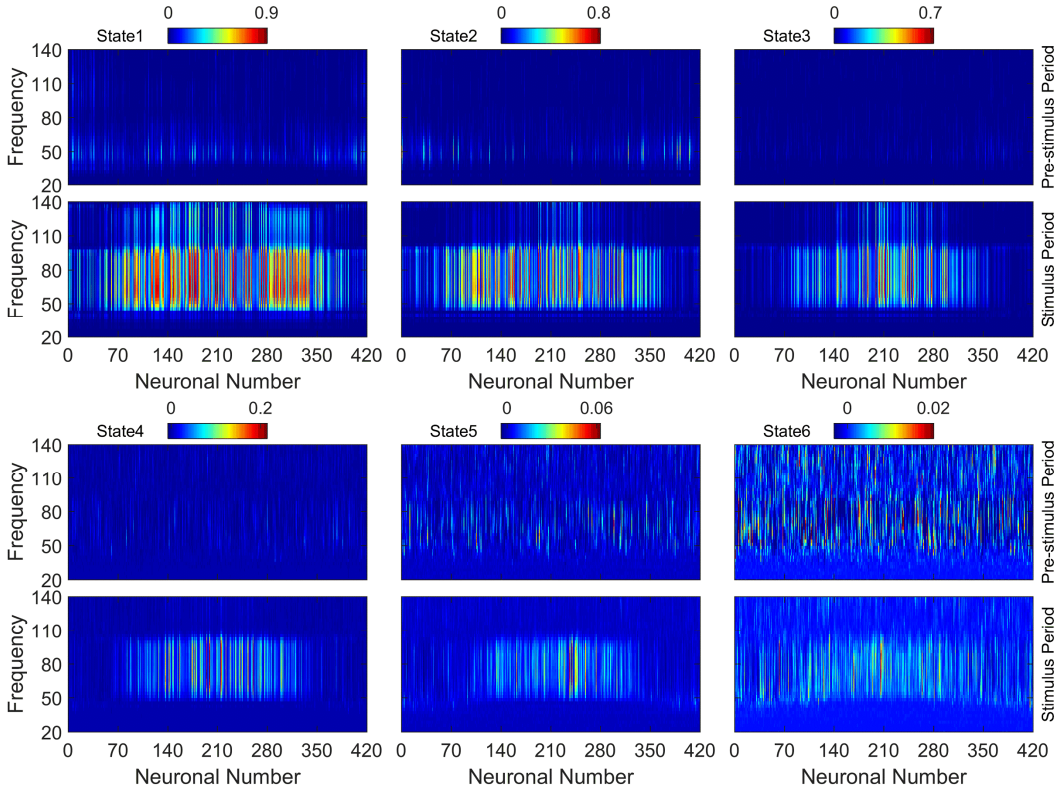

FIGURE 6. Distribution of PPC2 value for 420 individual neurons within a frequency range of 20-140 Hz for six network activity states during pre-stimulus and stimulus periods.

This article has been accepted for publication in a future issue of this journal, but has not been fully edited. Content may change prior to final publication. Citation information: DOI 10.1109/ACCESS.2018.2845301, IEEE Access

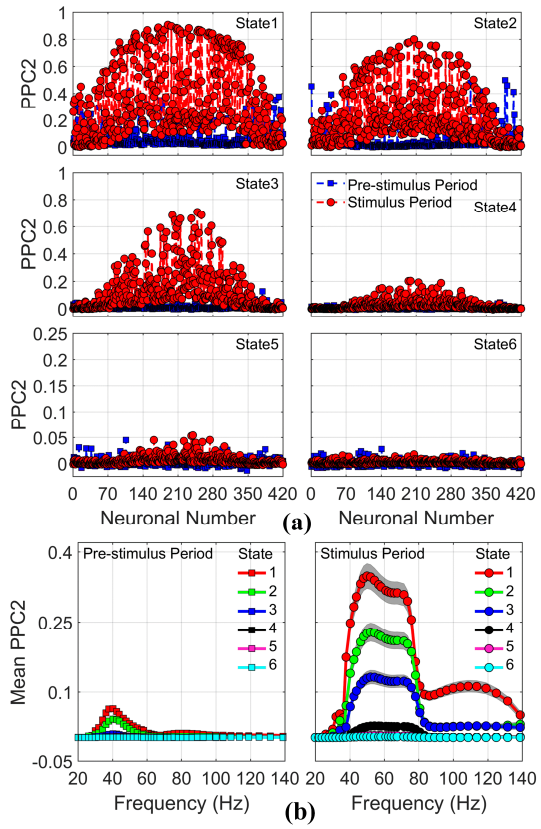

FIGURE 7. Distribution of PPC2 Value and Mean PPC2 Value. (a) PPC2 values of 420 individual neurons for six network activity states during pre-stimulus and stimulus periods. (b) Mean PPC2 value averaged across 420 neurons as a function of frequency 20-140 Hz for six network activity states during pre-stimulus and stimulus periods. The gray region represents 95% confidence interval.

leftward and rightward columns gradually decreased. It was consistent with electrophysiological recording studies that a certain degree of coherent activities is commonly observed within cortical orientation columns [60, 61]. From state1 to state6 during stimulus period, PPC2 values of 420 neurons decreased substantially and became more and more similar.

In addition, we further averaged the PPC2 values across 420 recorded neurons for both pre-stimulus and stimulus periods (Fig. 7(b)). The peak frequencies of the mean PPC2 values for both periods were compatible with peak frequencies of LFP power spectra. Besides, the significant region of the mean PPC2 values for stimulus period was located between 40 Hz and 80 Hz, a part of gamma frequency range. Moreover, in spite of no orientation stimulus during pre-stimulus period, there still existed slight excitatory oscillations in a gamma frequency range for state1 and state2, consistent with studies that synchrony even emerges in a baseline or resting state because of anatomical connectivity [30]. In addition, from state1 to state6 for both periods, the mean PPC2 values declined extensively.

As far as the 11th orientation column was concerned, it received 22 groups of excitatory inputs, the two strongest of which originated from its corresponding Poisson group with the largest Poisson rate, and the 11th column itself with the relatively highest neuronal excitation. The rest groups of excitatory inputs arose from other 20 columns with comparatively lower neuronal excitations. Besides, the synaptic connection strengths from the 11th column itself were the strongest, whereas the ones from other columns were considerably weak. Moreover, it has been recognized that the synaptic inhibition can significantly raise the leakiness of target neurons [24, 62]. Consequently, the 11th orientation column, as a target network with high neuronal excitation and strong intracolumn connectivity, was more likely to synchronize their spiking activities through coincidence detection [16], and thereby came up with relatively the largest PPC2 values.

E. RELATIONSHIPS FOR OSCILLATORY PHASE

In this section, we primarily investigated relationships of oscillatory phase with neuronal excitation measured by neuronal firing rate, as well as input strength characterized by Poisson rate and neuronal synaptic current power. The firing rate, Poisson rate and synaptic current power were all linear variables, whereas, spike-LFP phase was a circular variable. It was not suitable to use a general linear regression model to evaluate their relationships, which could not minimize circular error. Subsequently, we adopted a linear-circular regression model with an arctangent function, described in Equation (16) modified from [22]:

$$\overline{\Theta}_i = \mu + \alpha \tan^{-1}(\beta Y_i + b) + \varepsilon_i \qquad (16)$$

wherein $\overline{\Theta}_i$ was a spike-LFP phase for the ith neuron or the ith neuronal group. Y_i was firing rate or synaptic current power for an individual neuron, or Poisson rate for a neuronal group. The parameter β was the coefficient of regression slope to be estimated, and ε_i followed the von Mises distribution.

For the relationship between spike-LFP phase and neuronal firing rate during stimulus period, we only included the

TABLE 2. Parameter estimate of relationships for spike-LFP phase.

		State1	State2	State3	State4	State5	State6
FR	β	-0.659	-0.588	-1.089	\	\	\
	R squared	0.611	0.604	0.498	\	\	\
PR	β	-0.058	-0.054	-0.043	-0.038	-0.028	-0.040
	R squared	0.984	0.964	0.971	0.818	0.810	0.731
SCP	β	-0.029	-0.177	-0.300	-0.639	\	\
	R squared	0.834	0.797	0.698	0.464	\	\

FR: Firing Rate, PR: Poisson Rate, SCP: Synaptic Current Power

This article has been accepted for publication in a future issue of this journal, but has not been fully edited. Content may change prior to final publication. Citation information: DOI 10.1109/ACCESS.2018.2845301, IEEE Access

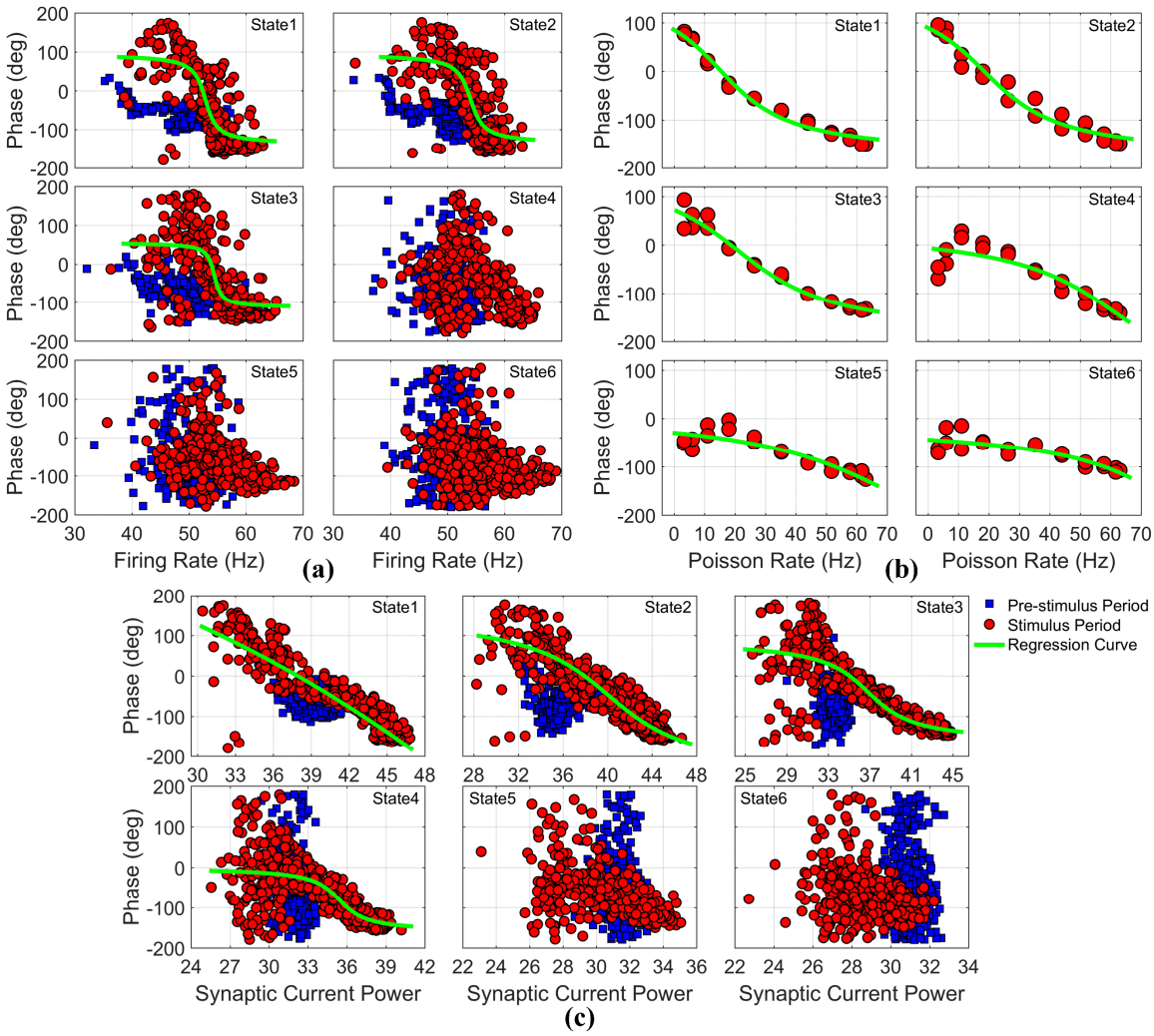

FIGURE 8. Relationships of Oscillatory Phase with Neuronal Excitation and Input Strength. (a) Spike-LFP phase for individual neurons as a function of neuronal firing rate. (b) Spike-LFP phase for 21 neuronal groups as a function of input Poisson rate. (c) Spike-LFP phase for 420 individual neurons as a function of neuronal synaptic current power.

neurons with PPC2 values under certain thresholds. The thresholds were {0.3, 0.22, 0.15, 0.03, 0.01, 0.005} for the six network activity states respectively. Because the neurons, with higher PPC2 values, were more likely to have similar point spike-LFP phases, which would be confined to certain phase intervals relative to the background oscillation. On the contrary, the neurons with lower PPC2 values probably had more random spike-LFP phases, therefore more suitable for the relationship quantification.

From state1 to state3 during stimulus period, three regression curves with declining slopes were estimated (Fig. 8(a)). According to Table. 2, the estimated coefficient β {-0.659, -0.588, -1.089} for the three regression curves were all negative. It indicated that the spike-LFP phase decreased as a function of neuronal firing rate, thus oscillatory phase decreased monotonically with neuronal excitation. It was in agreement with the gamma cycle hypothesis [21], theta-phase precession phenomenon [20], the gamma-phase shifting study [22], and other computational investigations [23, 24]. From state4 to state6, the spike-LFP phase became more and more scattered, and no obvious relationship was available between spike-LFP phase and neuronal firing rate.

For the relationship between spike-LFP phase and Poisson rate, we initially set the parameter α=2. Six regression curves, again with declining slopes, were estimated (Fig. 8(b)). Based on Table. 2, the estimated coefficient β {-0.058, -0.054, -0.043, -0.038, -0.028, -0.040} were all negative, suggesting that the spike-LFP phase decreased as a function of Poisson rate. In addition, as evident from Fig. 8(b), the decreasing speed between spike-LFP phase and Poisson rate became slower and slower from state1 to state6. Concerning with the relationship between spike-LFP phase and neuronal synaptic current power during stimulus period, four regression curves with declining slopes were evaluated (Fig. 8(c)). On the basis of Table. 2, the estimated β {-0.029, -0.177, -0.300, -0.639} for the regression curves were all negative as well, suggesting

This article has been accepted for publication in a future issue of this journal, but has not been fully edited. Content may change prior to final publication. Citation information: DOI 10.1109/ACCESS.2018.2845301, IEEE Access

that the spike-LPF phase decreased as a function of synaptic current power. When the noise parameter σ_n continued to increase, the quantifiable relationship disappeared as a result of increasingly dispersed spike-LFP phases. In summary, oscillatory phase was a monotonically decreasing function of neuronal input strength for general oscillatory state.

F. RELATIONSHIPS FOR PHASE SYNCHRONIZATION

In this section, we mainly investigated relationships of phase synchronization with neuronal excitation and neuronal input strength. Firstly, we measured the relationship between PPC2 value and neuronal excitation, represented by neuronal firing rate. The relationship was analyzed by a nonlinear regression model according to the equation below.

$$P_i = \alpha e^{\beta(Y_i+b)} + \varepsilon_i \quad (17)$$

where the term $P_i, i = 1,2,\dots,420$, was the PPC2 value for the i[th] neuron, Y_i the neuronal firing rate. The parameter β was the coefficient of regression slope to be estimated.

From state1 to state3, it was apparent that the scatter plot in each network activity state encompassed two peaks for pre-stimulus and stimulus periods respectively (Fig. 9(a)). Interestingly, the two peaks were around the peak frequencies of LFP power spectra for relevant periods. Around each peak point, we split the scatter data into two parts. Then, by virtue of Equation (17), we implemented nonlinear regression analyses and obtained a decreasing regression curve1 for pre-stimulus period, an increasing regression curve2 and a decreasing regression curve3 for stimulus period. The estimated values of coefficient β and R squared for the regression curves could be referred to Table. 3.

The two peaks of the scatter plot were also around the frequencies of neuronal raster plots and LFP oscillations. The peak firing rate approaching to oscillatory frequency implied that the neuron discharged regularly, with one spike discharging in each oscillatory cycle. It would have greater likelihood to obtain relatively stronger phase synchronization and higher PPC2 value. If the actual firing rate of a given neuron was smaller or larger than the peak firing rate, it meant there were no spikes or more than one spikes during some of oscillatory cycles. In consequence, the phase synchronization was correspondingly degraded, thus with relatively smaller PPC2 value. In general, the strength of phase synchronization, quantified by PPC2 value, increased gradually with neuronal excitation when neuronal firing rate was below oscillatory frequency. However, it decreased progressively with neuronal excitation when neuronal firing rate was above oscillatory frequency. Nevertheless, the regular relationship between phase synchronization and neuronal excitation no longer sustained as network oscillatory state became weak or nonexistent.

TABLE 3. Parameter estimate for relationship between PPC2 value and neuronal firing rate.

		State1	State2	State3
Curve1	β	-0.238880	-0.410256	\
	R squared	0.850	0.798	\
Curve2	β	1.314207	1.059148	2.356082
	R squared	0.814	0.653	0.560
Curve3	β	-0.277062	-0.263273	-0.263790
	R squared	0.721	0.509	0.333

Secondly, we investigated the relationship between PPC2 value and input strength, described by Poisson rate and neuronal synaptic current power. The relationships were generally analyzed by a regression method of linear curve estimation with the help of SPSS statistics software. Besides, we also utilized a nonlinear regression model to measure the relationship between PPC2 value and Poisson rate, through Equation (18).

$$P_i = \alpha + \beta \ln(Y_i + b) + \varepsilon_i \quad (18)$$

where the term $P_i, i = 1,2,\dots,21$, was the PPC2 value for the i[th] neuronal group, Y_i the Poisson rate. The parameter β was the regression coefficient to be estimated.

With respect to the relationship between PPC2 value and Poisson rate, two regression curves were estimated for each network activity state (Fig. 9(b)). The regression curve1 was obtained by the linear curve estimation method, the regression curve2 by Equation (18). According to Table. 4, the estimated values of coefficient β for the two regression curves in all six states were all positive, meaning that the PPC2 value increased as a function of Poisson rate. Furthermore, from state1 to state6, the parameter β of the linear curve1 decreased

TABLE 4. Parameter estimate for relationship between PPC2 value and neuronal input strength.

			State1	State2	State3	State4	State5	State6
Poisson Rate	Curve1	β	0.005600	0.004561	0.004376	0.000981	0.000222	0.000044
		R squared	0.542	0.692	0.889	0.962	0.815	0.792
	Curve2	β	0.139458	0.128161	0.938236	0.221610	0.056949	0.008845
		R squared	0.714	0.795	0.887	0.960	0.808	0.792
Synaptic Current Power		β	0.034101	0.024519	0.017970	0.005940	0.002182	0.000787
		R squared	0.799	0.859	0.885	0.965	0.805	0.740

This article has been accepted for publication in a future issue of this journal, but has not been fully edited. Content may change prior to final publication. Citation information: DOI 10.1109/ACCESS.2018.2845301, IEEE Access

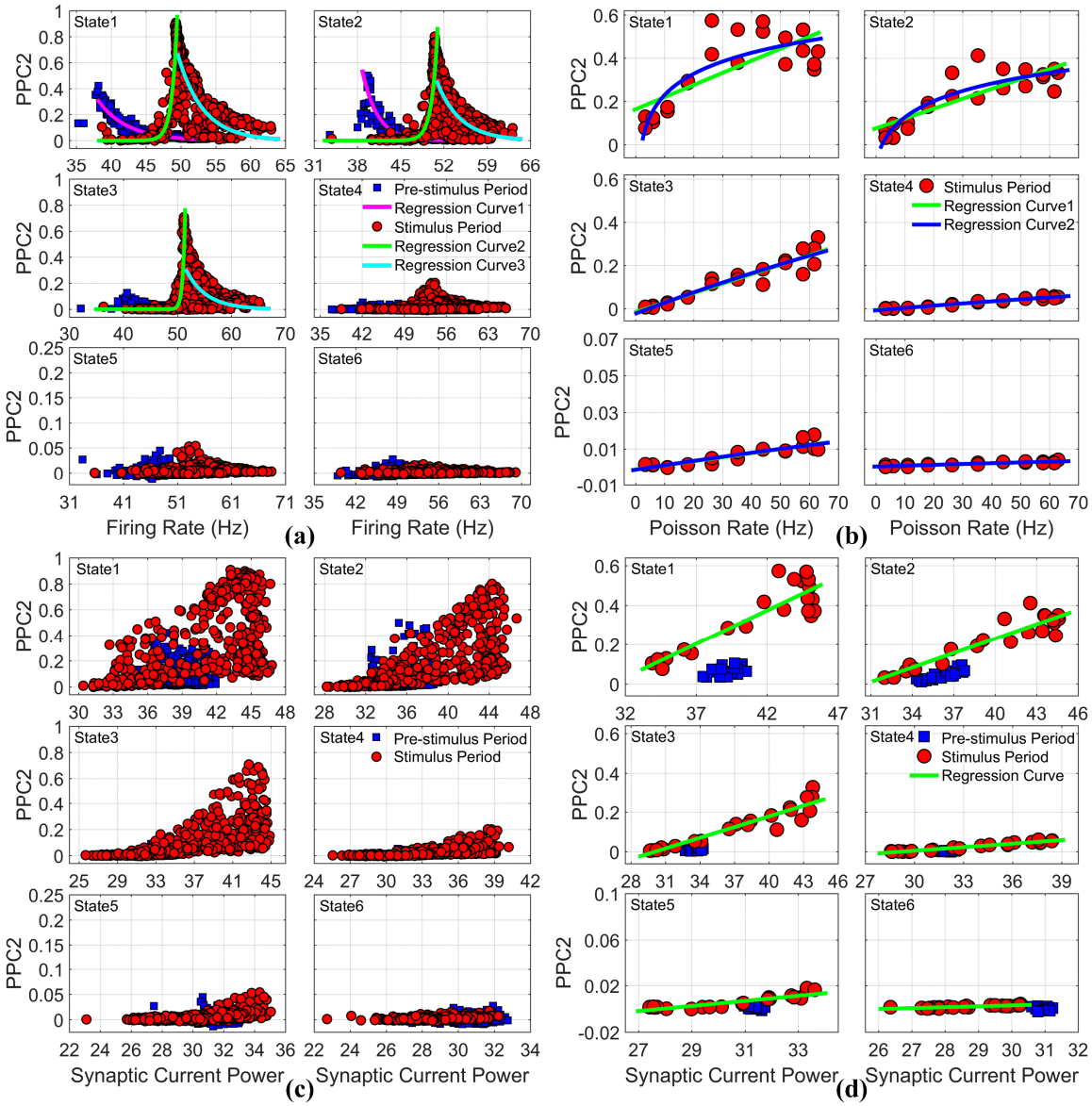

FIGURE 9. Relationships of Phase Synchronization with Neuronal Excitation and Input Strength. (a) PPC2 value for 420 individual neurons as a function of neuronal firing rate. (b) PPC2 value for 21 neuronal groups as a function of input Poisson rate. (c) PPC2 value for 420 individual neurons as a function of neuronal synaptic current power. (d) Similar to (c), but for 21 neuronal groups.

progressively, implying that the increasing speed between PPC2 value and Poisson rate became slower and slower.

With regard to the relationship between PPC2 value and neuronal synaptic current power, we firstly demonstrated PPC2 value in association with synaptic current power for 420 individual neurons (Fig. 9(c)). Unfortunately, little relationship information could be inferred from the scatter plot, in spite of gradually increasing trend for stimulus period. Then we quantified the relationship at a neuronal group level by the linear curve estimation method (Fig. 9(d)). Based on Table. 4, the estimated coefficient β for the six states were all positive, suggesting that PPC2 value increased as a function of neuronal synaptic current power. In addition, from state1 to state6, the coefficient β decreased gradually, indicating that the PPC2 value increased slower and slower with synaptic current power. In summary, the strength of phase synchronization increased monotonically with neuronal input strength for general oscillatory state.

G. TIME-RESOLVED ANALYSIS

In this section, we undertook time-resolved analyses of spike-LFP phase and PPC2 value for 420 sampled neurons. For state1 during pre-stimulus period, spike-LFP phases across 420 neurons were roughly similar despite certain variabilities (Fig. 10(a)). The PPC2 values across 420 neurons were relatively low (Fig. 10(b)). Besides, no matter spike-LFP phase or PPC2 value for the state1, there were variations at the beginning of pre-stimulus period. It was partly because the

This article has been accepted for publication in a future issue of this journal, but has not been fully edited. Content may change prior to final publication. Citation information: DOI 10.1109/ACCESS.2018.2845301, IEEE Access

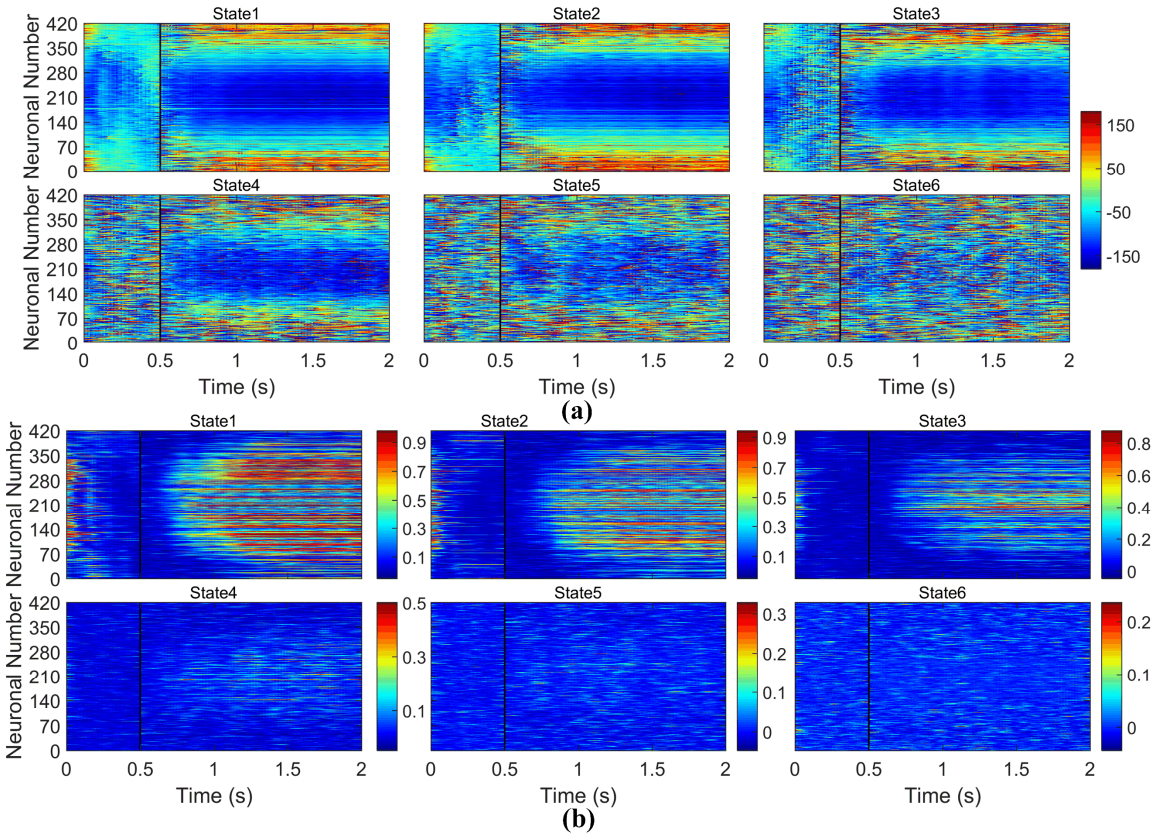

FIGURE 10. Time-Resolved Analyses for Spike-LFP Phase and PPC2 Value. (a) Evolution of spike-LFP phases of 420 recorded neurons across trial time for six network activity states. For each state, there are a 500 ms pre-stimulus period in the first part and a 1500 ms stimulus period in the second part. (b) Similar to (a), but for evolution of PPC2 values.

beginning session was sensitive to the influences imposed by input stimuli and neuronal activities of last trial. Furthermore, from state1 to state6 during this period, the spike-LFP phase fluctuated more and more extensively and the PPC2 values became increasingly smaller. However, they both retained similarity across 420 neurons.

For state1 during stimulus period, there were several attributes implied from Fig. 10. Firstly, the evolutions of spike-LFP phase and PPC2 value at most time points were in line with the distributions of spike phase and PPC2 value in previous sections. Secondly, at the beginning of stimulus period, the spike phases varied a lot, whereas the PPC2 values were considerably small and comparatively similar across 420 neurons. It was mainly attributable to the effect of stimulus onset transients [22], compatible with observations in a visual attention study [11]. Thirdly, the phases from two-side orientation columns fluctuated extensively, while the ones from middle columns were comparatively stable after the stimulus onset interval. However, the PPC2 values from the middle columns were comparatively larger and increased firstly, then followed by other nearby columns with lower PPC2 values. Therefore, less coherent or synchronized neuronal activities, with lower PPC2 values, were not effective in constraining neuronal spike times and thereby led to greater phase shifting. Fourthly, although neurons, from the same column, received similar Poisson input and possessed analogous synaptic connectivity, it was not uncommon that they would attain slightly heterogeneous neuronal activities, thus acquiring slightly different spike phases and PPC2 values within the same column. Furthermore, from strong oscillation to weak oscillation or non-oscillation, the middle columns with lower spike-LFP phases and higher PPC2 values became narrower and narrower, and both the spike phases and PPC2 values became increasingly similar across 420 neurons.

IV. CONCLUSION AND DISCUSSION

In order to investigate oscillatory phase, phase synchronization and their analytical relationships with neuronal excitation and input strength for different levels of oscillatory states, we constructed a spiking neural network with 21 Poisson groups to provide external thalamic inputs, and 21 columns to simulate orientation columns in primary visual cortex. Neurons in different columns were designated with different orientation preferences. The visual stimulation, data recording and subsequent spectral computation in our study were roughly analogous to the electrophysiological gamma-phase shifting experiment [22]. A leaky integrate-and-fire model was employed in the neuronal network on account of its biological plausibility and computational efficiency, which however could be substituted by the Hodgkin-Huxley

model or other neuronal models [63]. Besides, we explored properties of neuronal dynamics in six network activity states and for pre-stimulus and stimulus periods independently, and we also drew a parallel between them for comparison. In addition, a time-resolved analysis with a sliding window was also conducted for evolution of neuronal activities across trial time.

In our simulating experiment, the frequencies of spike raster and LFP oscillation, as well as the peak frequencies of LFP power spectra and mean PPC2 values were comparatively consistent during pre-stimulus and stimulus periods. Besides, the significant region of PPC2 values for 420 individual neurons was also in accordance with the significant region of mean PPC2 value during stimulus period, around a range of 45 Hz - 80 Hz. Altogether, the frequencies encountered above all belonged to the gamma frequency band, which thereby confirmed the existence of gamma neuronal rhythmicity in cortical network and were also in agreement with a wide spectrum of physiological experiments [5, 11, 22] and numerical investigations [19, 33, 52].

For a general oscillatory state, if the preferred orientation of a given column was the same as or similar to the input orientation, neurons within the column would receive larger Poisson input. Supplemented by stronger excitatory recurrent connections within this column, neurons from the column would acquire higher neuronal excitations and firing rates. It could in turn overcome synchronous inhibitions firstly, discharge earlier and come up with smaller and similar spike-LFP phases, but larger PPC2 values. In particular, the spike-LFP phase decreased monotonically with neuronal excitation and input strength. However, the PPC2 value increased with neuronal excitation in the first part and decreased in the second part, but it increased constantly as a function of input strength. The investigation of oscillatory phase in our study confirmed the gamma cycle hypothesis [21], also consistent with the theta-phase precession phenomenon [20] and the gamma-phase shifting study [22]. When the network activity state transformed gradually from strong oscillation to weak oscillation or non-oscillation, spike-LFP phases became more and more scattered and PPC2 values decreased significantly. Furthermore, the reliable and quantifiable relationships of the spike-LFP phase and PPC2 value with neuronal excitation and input strength became increasingly unstable and finally nonexistent.

Despite the consistency between our research and the gamma-phase shifting study [22], there are still several subtle differences. Firstly, the neuronal excitation in our simulation was represented by neuronal firing rate, whereas the one in the phase shifting study was described by spike density, a quantity of temporally neighboring spikes on a short timescale [22]. Secondly, oscillatory phase in our study was denoted by spike-LFP phase, averaging point spike-LFP phases across trials. However, the one in the phase shifting experiment was directly the point spike-LFP phase itself. However, there was also mean spike-LFP phase for spike density percentile in the phase shifting study [22]. Lastly, we quantified phase synchronization by PPC2 measure, while PLV approach was adopted in the phase shifting study [22]. Especially, the PPC measure was a bias-free method, the population statistic of which was equivalent to the population statistic of the squared PLV [29, 35].

Several computational studies have derived similar outcomes about oscillatory phase and its relationship with external input [23, 24]. However, the oscillatory phase employed in these studies was generally obtained in time domain, as opposed to implementing spectrum computation in frequency domain as physiological experiments. In a computational study, synchronous neuronal activities were modeled as a periodic sequence of Gaussian peaks, and the phases were directly defined relative to a reference time of underlying oscillations [23]. In another computational study, stimulus inputs were provided by sinusoidal signals, and the phases were established relative to the sinusoidal signals [24]. However, the spike-LFP phase in our simulation was derived from spike-triggered LFP spectrum through Fourier transformation in frequency domain, which was much similar to physiological experimental methods.

Accumulated evidences have suggested that a possible functional role of oscillatory phase in sensory feature coding. The oscillation cycle, like the gamma cycle, is proposed to serve as a temporal reference frame. The stimulus attribute and neuronal functional architecture determine the level of neuronal excitation, which in turn defines the time and phase of a neuronal spike relative to the surrounding cycle [21]. Therefore, the relationship quantifications for oscillatory phase with neuronal excitation and input strength are important for feature coding and sensory representation. Besides, the interaction strength between neuronal groups is also dependent on their relative phase [5, 16, 52]. In addition to phase coding, there is also firing rate coding [64]. It is generally utilized either exclusively without phase coding [65], or concurrently with phase coding [66]. It is assumed that firing rate coding is responsible for discrete properties of input stimuli, whereas phase coding is used for tagging relationships for stimulus properties and neuronal firing rates, and faster at identifying sensory information than rate coding[17, 64].

Thus far, the strength of neuronal synchronization is generally used as a quantification for determining flexible interactions and communications among neuronal groups on the grounds of the CTC hypothesis [7, 31]. A more coherent or synchronous excitatory input is known to have a competitive advantage over less coherent ones to entrain a target network with inhibitory interneurons [62], and the effectiveness of signal or information gating is dependent on the degree of neuronal synchronization [23]. Subsequently, the relationships of phase synchronization with neuronal excitation and input strength in our model are useful to guarantee flexible and dynamic functional connectivity among neuronal groups so as to implement cognitive functions of

neuronal communication, signal routing and selective attention.

For further investigation, we should explore the computational mechanism of oscillatory phase and phase synchronization at different frequencies [49, 57] and with different synaptic transmission delays among remote neuronal populations [19] according to a new CTC hypothesis [31]. Meanwhile, we should also investigate the computational principle of phase-amplitude and phase-phase coupling between faster and lower neuronal oscillations [3, 6, 17].

REFERENCES

[1] C. M. Gray, P. Konig, A. K. Engel, and W. Singer,"Oscillatory responses in cat visual cortex exhibit inter-columnar synchronization which reflects global stimulus properties," *Nature*, vol. 338, no. 6213, pp. 334-337, Mar. 1989.

[2] Y. B. Saalmann, M. A. Pinsk, L. Wang, X. Li, and S. Kastner,"The pulvinar regulates information transmission between cortical areas based on attention demands," *Science*, vol. 337, no. 6095, pp. 753-756, Aug. 2012.

[3] K. M. Igarashi, L. Lu, L. L. Colgin, M. Moser, and E. I. Moser,"Coordination of entorhinal-hippocampal ensemble activity during associative learning," *Nature*, vol. 510, no. 7503, pp. 143-147, Jun. 2014.

[4] T. Spellman, M. Rigotti, S. E. Ahmari, S. Fusi, J. A. Gogos, and J. A. Gordon,"Hippocampal-prefrontal input supports spatial encoding in working memory," *Nature*, vol. 522, no. 7556, pp. 309-314, Jun. 2015.

[5] T. Womelsdorf, J. Schoffelen, R. Oostenveld, W. Singer, R. Desimone, A. K. Engel, and P. Fries,"Modulation of neuronal interactions through neuronal synchronization," *Science*, vol. 316, no. 5831, pp. 1609-1612, Jun. 2007.

[6] R. T. Canolty, E. Edwards, S. S. Dalal, M. Soltani, S. S. Nagarajan, H. E. Kirsch, M. S. Berger, N. M. Barbaro, and R. T. Knight,"High gamma power is phase-locked to theta oscillations in human neocortex," *Science*, vol. 313, no. 5793, pp. 1626-1628, Sep. 2006.

[7] P. Fries,"A mechanism for cognitive dynamics: neuronal communication through neuronal coherence," *Trends Cogn Sci*, vol. 9, no. 10, pp. 474-480, Oct. 2005.

[8] T. Akam and D. M. Kullmann,"Oscillatory multiplexing of population codes for selective communication in the mammalian brain," *Nat Rev Neurosci*, vol. 15, no. 2, pp. 111-122, Feb. 2014.

[9] W. Singer and C. M. Gray,"Visual feature integration and the temporal correlation hypothesis," *Annu. Rev. Neurosci.*, vol. 18, no. 1, pp. 555-586, Jan. 1995.

[10] N. Brunet, C. A. Bosman, M. Roberts, R. Oostenveld, T. Womelsdorf, P. De Weerd, and P. Fries,"Visual cortical gamma-band activity during free viewing of natural images," *Cereb Cortex*, vol. 25, no. 4, pp. 918-926, Apr. 2015.

[11] P. Fries, J. H. Reynolds, A. E. Rorie, and R. Desimone,"Modulation of oscillatory neuronal synchronization by selective visual attention," *Science*, vol. 291, no. 5508, pp. 1560-1563, Feb. 2001.

[12] D. Baldauf and R. Desimone,"Neural mechanisms of object-based attention," *Science*, vol. 344, no. 6182, pp. 424-427, Apr. 2014.

[13] J. Fell and N. Axmacher,"The role of phase synchronization in memory processes," *Nat Rev Neurosci*, vol. 12, no. 2, pp. 105-118, Feb. 2011.

[14] J. A. Cardin, M. Carlen, K. Meletis, U. Knoblich, F. Zhang, K. Deisseroth, L. Tsai, and C. I. Moore,"Driving fast-spiking cells induces gamma rhythm and controls sensory responses," *Nature*, vol. 459, no. 7247, pp. 663-667, Jun. 2009.

[15] G. Buzsaki and X. J. Wang,"Mechanisms of Gamma Oscillations," *Annu. Rev. Neurosci.*, vol. 35, no. 1, pp. 203-225, Mar. 2012.

[16] P. Fries,"Neuronal gamma-band synchronization as a fundamental process in cortical computation," *Annu. Rev. Neurosci.*, vol. 32, no. 1, pp. 209-224, Jul. 2009.

[17] C. A. Bosman, C. S. Lansink and C. M. A. Pennartz,"Functions of gamma-band synchronization in cognition: from single circuits to functional diversity across cortical and subcortical systems," *Eur J. Neurosci*, vol. 39, no. 11, pp. 1982-1999, Jun. 2014.

[18] M. A. Whittington, R. D. Traub and J. G. Jefferys,"Synchronized oscillations in interneuron networks driven by metabotropic glutamate receptor activation," *Nature*, vol. 373, no. 6515, pp. 612-615, Feb. 1995.

[19] A. Barardi, B. Sancristobal and J. Garcia-Ojalvo,"Phase-coherence transitions and communication in the gamma range between delay-coupled neuronal populations," *Plos Comput. Biol.*, vol. 10, no. 7, pp. e1003723, Jul. 2014.

[20] J. O'Keefe and M. L. Recce,"Phase relationship between hippocampal place units and the EEG theta rhythm," *Hippocampus*, vol. 3, no. 3, pp. 317-330, Jul. 1993.

[21] P. Fries, D. Nikolic and W. Singer,"The gamma cycle," *Trends Neurosci*, vol. 30, no. 7, pp. 309-316, Jun. 2007.

[22] M. Vinck, B. Lima, T. Womelsdorf, R. Oostenveld, W. Singer, S. Neuenschwander, and P. Fries,"Gamma-phase shifting in awake monkey visual cortex," *J. Neurosci*, vol. 30, no. 4, pp. 1250-1257, Jan. 2010.

[23] P. H. Tiesinga and T. J. Sejnowski,"Mechanisms for phase shifting in cortical networks and their role in communication through coherence," *Front. Hum. Neurosci.*, vol. 4, no. 196, Nov. 2010.

[24] S. Gielen, M. Krupa and M. Zeitler,"Gamma oscillations as a mechanism for selective information transmission," *Biol Cybern*, vol. 103, no. 2, pp. 151-165, Aug. 2010.

[25] M. A. Montemurro, M. J. Rasch, Y. Murayama, N. K. Logothetis, and S. Panzeri,"Phase-of-firing visual stimuli in coding of natural primary visual cortex," *Curr Biol*, vol. 18, no. 5, pp. 375-380, Mar. 2008.

[26] M. Smear, R. Shusterman, R. O'Connor, T. Bozza, and D. Rinberg,"Perception of sniff phase in mouse olfaction," *Nature*, vol. 479, no. 7373, pp. 397-400, Nov. 2011.

[27] M. Siegel, M. R. Warden and E. K. Miller,"Phase-dependent neuronal coding of objects in short-term memory," *P. Natl Acad Sci Usa*, vol. 106, no. 50, pp. 21341-21346, Dec. 2009.

[28] L. L. Colgin, T. Denninger, M. Fyhn, T. Hafting, T. Bonnevie, O. Jensen, M. Moser, and E. I. Moser,"Frequency of gamma oscillations routes flow of information in the hippocampus," *Nature*, vol. 462, no. 7271, pp. 353-357, Nov. 2009.

[29] M. Vinck, F. P. Battaglia, T. Womelsdorf, and C. Pennartz,"Improved measures of phase-coupling between spikes and the Local Field Potential," *J. Comput Neurosci*, vol. 33, no. 1, pp. 53-75, Aug. 2012.

[30] A. Z. Harris and J. A. Gordon,"Long-range neural synchrony in behavior," *Annu. Rev. Neurosci.*, vol. 38, no. 1, pp. 171-194, Jul. 2015.

[31] P. Fries,"Rhythms for Cognition: Communication through Coherence," *Neuron*, vol. 88, no. 1, pp. 220-235, Oct. 2015.

[32] J. P. Lachaux, E. Rodriguez, J. Martinerie, and F. J. Varela,"Measuring phase synchrony in brain signals," *Hum Brain Mapp*, vol. 8, no. 4, pp. 194-208, Nov. 1999.

[33] M. Zeitler, P. Fries and S. Gielen,"Assessing neuronal coherence with single-unit, multi-unit, and local field potentials," *Neural Comput*, vol. 18, no. 9, pp. 2256-2281, Sep. 2006.

[34] M. Zeitler, P. Fries and S. Gielen,"Biased competition through variations in amplitude of gamma-oscillations," *J. Comput Neurosci*, vol. 25, no. 1, pp. 89-107, Aug. 2008.

[35] M. Vinck, M. van Wingerden, T. Womelsdorf, P. Fries, and C. M. A. Pennartz,"The pairwise phase consistency: A bias-free measure of rhythmic neuronal synchronization," *Neuroimage*, vol. 51, no. 1, pp. 112-122, May. 2010.

[36] P. Tiesinga and T. J. Sejnowski,"Cortical Enlightenment: Are Attentional Gamma Oscillations Driven by ING or PING?" *Neuron*, vol. 63, no. 6, pp. 727-732, Sep. 2009.

[37] X. X. Jia, D. J. Xing and A. Kohn,"No Consistent Relationship between Gamma Power and Peak Frequency in Macaque Primary Visual Cortex," *J. Neurosci*, vol. 33, no. 1, pp. 17-25, Jan. 2013.

[38] N. Brunel and D. Hansel,"How noise affects the synchronization properties of recurrent networks of inhibitory neurons," *Neural Comput*, vol. 18, no. 5, pp. 1066-1110, May. 2006.

[39] S. Ostojic, N. Brunel and V. Hakim,"Synchronization properties of networks of electrically coupled neurons in the presence of noise and heterogeneities," *J. Comput Neurosci*, vol. 26, no. 3, pp. 369-392, Jun. 2009.

[40] T. P. Vogels, H. Sprekeler, F. Zenke, C. Clopath, and W. Gerstner,"Inhibitory Plasticity Balances Excitation and Inhibition in Sensory Pathways and Memory Networks," *Science*, vol. 334, no. 6062, pp. 1569-1573, Dec. 2011.
[41] R. Brette,"Computing with Neural Synchrony," *Plos Comput. Biol.*, vol. 8, no.6, pp. e10025616, Jun. 2012.
[42] R. J. Douglas and K. Martin,"Neuronal circuits of the neocortex," *Annu. Rev. Neurosci.*, vol. 27, pp. 419-451, Jul. 2004.
[43] H. Hu, J. Gan and P. Jonas,"Fast-spiking, parvalbumin(+) GABAergic interneurons: From cellular design to microcircuit function," *Science*, vol. 345, no. 6196, pp. 1255263, Aug. 2014.
[44] D. Ferster and K. D. Miller,"Neural mechanisms of orientation selectivity in the visual cortex," *Annu. Rev. Neurosci.*, vol. 23, no. 1, pp. 441-471, Mar. 2000.
[45] D. H. Hubel and T. N. Wiesel,"Receptive fields, binocular interaction and functional architecture in the cat's visual cortex," *The Journal of Physiology*, vol. 160, no. 1, pp. 106-154, Jan. 1962.
[46] R. C. Reid,"From Functional Architecture to Functional Connectomics," *Neuron*, vol. 75, no. 2, pp. 209-217, Jul. 2012.
[47] D. C. Somers, S. B. Nelson and M. Sur,"An emergent model of orientation selectivity in cat visual cortical simple cells," *J. Neurosci*, vol. 15, no. 8, pp. 5448-5465, Aug. 1995.
[48] H. Markram, M. Toledo-Rodriguez, Y. Wang, A. Gupta, G. Silberberg, and C. Wu,"Interneurons of the neocortical inhibitory system," *Nat Rev Neurosci*, vol. 5, no. 10, pp. 793-807, Oct. 2004.
[49] B. Sancristobal, R. Vicente and J. Garcia-Ojalvo,"Role of frequency mismatch in neuronal communication through coherence," *J. Comput Neurosci*, vol. 37, no. 2, pp. 193-208, Oct. 2014.
[50] M. Kaiser, C. C. Hilgetag and A. van Ooyen,"A Simple Rule for Axon Outgrowth and Synaptic Competition Generates Realistic Connection Lengths and Filling Fractions," *Cereb Cortex*, vol. 19, no. 12, pp. 3001-3010, Dec. 2009.
[51] T. Akam and D. M. Kullmann,"Oscillations and filtering networks support flexible routing of information," *Neuron*, vol. 67, no. 2, pp. 308-320, Jul. 2010.
[52] A. Buehlmann and G. Deco,"Optimal information transfer in the cortex through synchronization," *Plos Comput. Biol.*, vol. 6, no. e10009349, pp. e1000934, Sep. 2010.
[53] D. F. M. Goodman and R. Brette,"The brian simulator.," *Front. Neurosci.-Switz*, vol. 3, no. 2, pp. 192-197, Sep. 2009.
[54] R. Oostenveld, P. Fries, E. Maris, and J. Schoffelen,"FieldTrip: Open source software for advanced analysis of MEG, EEG, and invasive electrophysiological data.," *Comput. Intel. Neurosc.*, vol. 2011, pp. 156869-156869, Jan. 2011.
[55] A. Mazzoni, S. Panzeri, N. K. Logothetis, and N. Brunel,"Encoding of naturalistic stimuli by local field potential spectra in networks of excitatory and inhibitory neurons," *Plos Comput. Biol.*, vol. 4, no. 12, pp. e1000239, Dec. 2008.
[56] S. Ray and J. H. Maunsell,"Differences in gamma frequencies across visual cortex restrict their possible use in computation," *Neuron*, vol. 67, no. 5, pp. 885-896, Sep. 2010.
[57] M. J. Roberts, E. Lowet, N. M. Brunet, M. Ter Wal, P. Tiesinga, P. Fries, and P. De Weerd,"Robust gamma coherence between macaque V1 and V2 by dynamic frequency matching," *Neuron*, vol. 78, no. 3, pp. 523-536, May. 2013.
[58] C. A. Bosman, J. Schoffelen, N. Brunet, R. Oostenveld, A. M. Bastos, T. Womelsdorf, B. Rubehn, T. Stieglitz, P. De Weerd, and P. Fries,"Attentional Stimulus Selection through Selective Synchronization between Monkey Visual Areas," *Neuron*, vol. 75, no. 5, pp. 875-888, Sep. 2012.
[59] M. Bartos, I. Vida and P. Jonas,"Synaptic mechanisms of synchronized gamma oscillations in inhibitory interneuron networks," *Nat Rev Neurosci*, vol. 8, no. 1, pp. 45-56, Jan. 2007.
[60] R. Eckhorn, R. Bauer, W. Jordan, M. Brosch, W. Kruse, M. Munk, and H. J. Reitboeck,"Coherent oscillations: a mechanism of feature linking in the visual cortex? Multiple electrode and correlation analyses in the cat," *Biol Cybern*, vol. 60, no. 2, pp. 121-130, Dec. 1988.
[61] M. Tsodyks, T. Kenet, A. Grinvald, and A. Arieli,"Linking spontaneous activity of single cortical neurons and the underlying functional architecture," *Science*, vol. 286, no. 5446, pp. 1943-1946, Dec. 1999.
[62] C. Boergers and N. J. Kopell,"Gamma oscillations and stimulus selection," *Neural Comput*, vol. 20, no. 2, pp. 383-414, Feb. 2008.
[63] A. L. Hodgkin and A. F. Huxley,"A quantitative description of membrane current and its application to conduction and excitation in nerve.," *The Journal of physiology*, vol. 117, no. 4, pp. 500–544, Aug. 1952.
[64] M. Ainsworth, S. Lee, M. O. Cunningham, R. D. Traub, N. J. Kopell, and M. A. Whittington,"Rates and rhythms: a synergistic view of frequency and temporal coding in neuronal networks," *Neuron*, vol. 75, no. 4, pp. 572-583, Aug. 2012.
[65] P. R. Roelfsema, V. Lamme and H. Spekreijse,"Synchrony and covariation of firing rates in the primary visual cortex during contour grouping," *Nat Neurosci*, vol. 7, no. 9, pp. 982-991, Sep. 2004.
[66] J. Biederlack, M. Castelo-Branco, S. Neuenschwander, D. W. Wheeler, W. Singer, and D. Nikolic,"Brightness induction: Rate enhancement and neuronal synchronization as complementary codes," *Neuron*, vol. 52, no. 6, pp. 1073-1083, Dec. 2006.